Discrete element modelling of flexible fibre packing

Paul Langston *, Andrew R. Kennedy, Hannah Constantin

Faculty of Engineering, Manufacturing Division, University of Nottingham, University Park, Nottingham NG7 2RD, UK

ARTICLE INFO

ABSTRACT

This paper presents Discrete Element Model simulations of packing of non-cohesive flexible fibres in a cylindrical vessel. No interstitial fluid effects are modelled. Each fibre-particle is modelled as a series of connected sphero-cylinders. In an initial study each particle is modelled a single rigid sphero-cylinder; the method has been used before but this study considers higher aspect ratios up to 30. This posed some modelling challenges in terms of stability which were overcome by imposing limits on the particle angular velocity. The results show very good agreement with experimental data in the literature and more detailed in-house experiments for packing volume fraction. Model results on particle orientation are also shown. The model is developed to include flexibility by connecting sphero-cylinders as sub-elements to describe a particle. Some basic tests are shown for the joint model that connects the sub-elements. The simulation results show similar trends to the rigid particle results with increased packing fraction. The effects of number of sub-elements, joint properties and contact friction are examined. The model has the potential for predicting packing of fibrous particles and fibre bundles relevant to the preparation of preforms for the production of discontinuously-reinforced polymer, ceramic and metallic matrix composites.

1. Introduction

Modelling of the packing of fibres is of high interest to the fabrication of discontinuously-reinforced composite materials. For the example of metal matrix composites, their preparation can be affected by the pressure-assisted infiltration of a packed ceramic fibre "preform" with a liquid metal. It is of significant benefit to be able to predict the packing behaviour of the fibres (or bundles of fibres) which form a rigid preform and hence which will dictate both the processing conditions required for successful infiltration but also the structure and properties in the final composite part. Fig. 1 shows an example of a metal matrix composite made by infiltration of a preform of discontinuous carbon fibres as well as the typical architecture of a "mat" made from carbon fibres.

Altering the aspect ratio of the fibre is one of the simplest ways in which the packing fraction might be varied and means that through appropriate chopping or milling, the volume fraction of fibres in the rigid preform can be tailored to suit the mechanical properties required. Whilst improved packing, and to some extent easier interspersion of the metal and fibre phases occurs as the fibre aspect ratio decreases, this is to the detriment of the efficiency of load transfer and hence the final properties. For typical metal–ceramic systems (with 20–50 vol.% reinforcement), a minimum aspect ratio of roughly 20 is targeted to achieve effective load transfer to the reinforcement [1]. Examples of applications of metal matrix composites are described in [2,3] and a commercial example is shown at <http://www.cmt-Ltd.com/index.html>.

Simple geometrical models, such as that by Parkhouse and Kelly [4], have been developed for similar treatments in polymer composite systems and show the interdependence between fibre aspect ratio and packing fraction (for example a packing of 30 vol.% of the available space being predicted for fibres with an aspect ratio of 20). Development of these simple models to finite volumes, to incorporate additional friction and cohesion terms and with quantification of the orientation distribution of the fibres in the vessel will greatly enhance the insight that is possible through this modelling approach.

Section 2 summarises the DEM technique which is widely used to model granular flow and packing [5–8]. Most applications model spherical particles but there are an increasing number which model non-spheres such as hemi-spherical ended cylinders. This paper models packing of such sphero-cylinders, and also flexible fibres modelled by connected sphero-cylinders.

Section 3 describes an initial study which modelled each particle as a single rigid sphero-cylinder with aspect ratios up to 30 [9]. This posed some modelling challenges in terms of stability which

---

* Corresponding author. Tel.: +44 115 951 4177.
E-mail address: p.langston@nottingham.ac.uk (P. Langston).

were overcome by imposing limits on the particle angular velocity. Model results are compared with theory and experiments.

Section 2.4 describes how the model is developed to include flexibility by connecting sphero-cylinders as sub-elements to describe a particle, and shows some basic tests for the joint model. Section 4 shows the results of packing fraction dependent on particle properties for the flexible particles. Section 5 summarises the conclusions.

2. Discrete Element Model (DEM)

2.1. DEM sphere method

The Discrete Element Method applied to spheres is well established as a reasonably realistic tool, in a wide range of engineering disciplines, for modelling packing and flow of granular materials; Asmar et al. [8] describes the fundamentals of this method as applied by code developed in-house at Nottingham; since these are widely documented the details are not reproduced here, simply a summary. It applies an explicit time stepping approach to numerically integrate the translational and rotational motion of each particle from the resulting forces and moments acting on them at each timestep. The inter-particle and particle wall contacts are modelled using the linear spring–dashpot–slider analogy. Contact forces are modelled in the normal and tangential directions with respect to the line connecting the particles centres. Particle elastic stiffness is set so sphere "overlap" is not significant and moderate contact damping is applied. Particle cohesion can also be modelled but is assumed to be negligible in the current study. The translational and rotational motion of each particle is modelled using a half step leap-frog Verlet numerical integration scheme to update particle positions and velocities. Near-neighbour lists are used to increase the computational efficiency of determining particle contacts and a zoning method is used each time the list is composed; that is the system is divided into cubic regions, each particle centre is within one zone, and potential contacting particles are within the same or next-door neighbour zones. Full details are given in Asmar et al. [8].

Rolling friction is often modelled as an angular torque arising from the elastic hysteresis loss or viscous dissipation [10], this enables more realistic rolling behaviour in DEM spheres (but is not applied here to the fibres described later). Further useful references which consider determination of contact parameters for DEM and scaling laws are in [11,12].

2.2. DEM for non-spherical particles

Developing DEM to model non-spheres is a significant issue. Various methods are used as reviewed in [5] and briefly in [7]. These include sphero-cylinders, super-quadrics, sphero-discs, polyhedra and combined finite–discrete element (FEM/DEM) methods. These studies show that particle shape can be very significant. For fibre shaped particles the following references are particularly noted.

Cruz Hidalgo et al. [13] models rods in an experimental and numerical study of stress propagation in granular packings; the contact force distribution is affected by particle aspect ratio. Hidalgo et al. [14] investigate the effect of particle cohesion in packing simulation of rods in 2D; the cohesion tends towards more open packing and breaks up the horizontal alignment of non-cohesive packings. Using clumped spheres is another method and has the advantage of simplicity and versatility. For example Nan et al. [15] models packing of long rigid fibres, straight and curved; the packing structure is investigated for different aspect ratio and
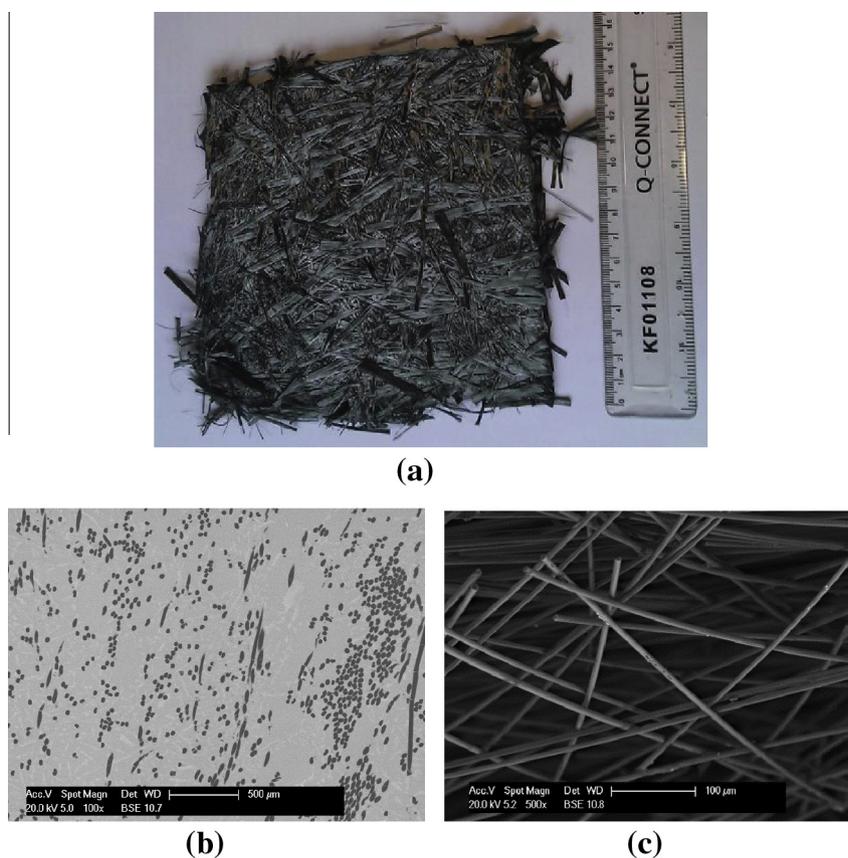

(a)

(b)

(c)

Fig. 1. (a) Example of directed carbon fibre preform; (b) an Al alloy composite containing discontinuous carbon fibres; (c) a preform of carbon fibres.

curl index. Guo et al. [16] describes a DEM model for flexible fibres using a bonded sphere model; this considers in detail the advantages and disadvantages of spheres vs. cylinders in such an approach. The bond model includes stretching, bending and twisting. Detailed validation is included and it recommends that the model time step should be less than the time for an axial stress wave to travel a single bond length. This reference is particularly relevant for the modelling here in Section 4. Other related references include [17,18] which model cracking in fibre reinforced composites.

2.3. DEM "sphero-cylinder" method

This technique is briefly mentioned in the review by Džiugys and Peters [5]. The particle is described by a cylinder with hemispherical ends of the same radius. The advantage of this geometry is that an essentially analytical method can be used to calculate contact location and contact normal force direction. The algorithm below was developed in [6] and has been used in the current study to determine particle–particle contact point, overlap and normal direction to contact.

- Each particle has an associated enclosing sphere with same centre as particle; check for enclosing sphere contact between particles, exit if none.
- Calculate the shortest distance pq between the two lines for each cylinder axis.
- If p and q lie within the particle line segments, check for cylinder–cylinder contact.
- Else if p or q lie within the particle line segments, check for cylinder-hemisphere contact.
- Else if neither p or q lie within the particle line segments, check for hemisphere–hemisphere contact.

From p and q and particle radii, determine contact details.

2.4. DEM flexible sphero-cylinder method

This model is the same as in Section 2.3 above except that each particle is modelled by a number of equal sized sub-elements of sphero-cylinders connected sequentially at the spheres. An example of a particle under a test algorithm is shown in Fig. 2. For convenience it always uses an odd number of elements so there is a reference central element. As a particle deforms a reaction is set up at each joint affecting the connected sub-elements with three components:
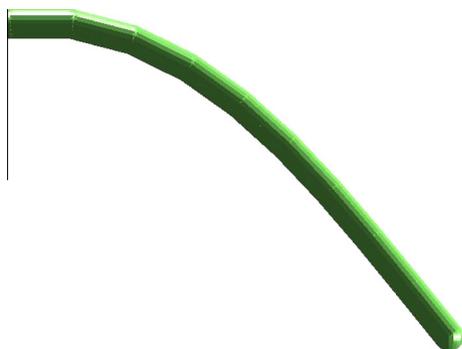
- a translational force to restore sphere centres to the same position; this uses a linear model with the same stiffness as the particle–particle contact;
- a bending moment proportional to the angular deformation in connected-particle-element plane per unit particle element length;
- a torsional moment proportional to the angular twist per unit particle element length.

Note: no failure mechanism (plastic or rupture) is modelled, but the model outputs warning messages if the deformations exceed user defined values. Some bending and torsional damping is included in proportion to the relative angular velocity between the elements.

For each potential particle–particle interaction every potential inter-particle sub-element interaction is considered. No cohesion is modelled here so only when sub-elements are in contact is there a resulting force and moment. At present the model assumes that there will not be "excessive bending or torsion" so sub-elements within a particle are taken as not interacting except for the joint response as detailed above. (At present no use is made of near-neighbour lists and particle zoning to speed up determination of which elements interact.)

Appendix A shows the equations used here to model joint bending stiffness and torsional stiffness.

Fig. 2 illustrates a "bending test" for a single particle to help check the code for bugs. Fig. 3 shows a similar example for torsion. The model stiffness and damping values are selected for reasonably visible responses and are somewhat softer than in the application in Section 4.

3. Application of DEM to rigid straight fibre packing

3.1. Scenario and principal data

The above algorithm for single sphero-cylinders (Section 2.3) is used here to model dropping rigid straight fibre particles into a cylindrical vessel to estimate the packing fraction. Particle–particle forces are modelled with a linear spring–dashpot–slider analogy. Cohesion and rolling friction coefficients are set to zero and no interstitial fluid is included. Particle–wall contact forces are similarly modelled. Constant gravity is modelled. A "softened" particle normal stiffness is used as is usual in DEM flow/packing simulations to allow a reasonable simulation timestep, but stiff enough to prevent any significant overlap and artificial effects on packing;
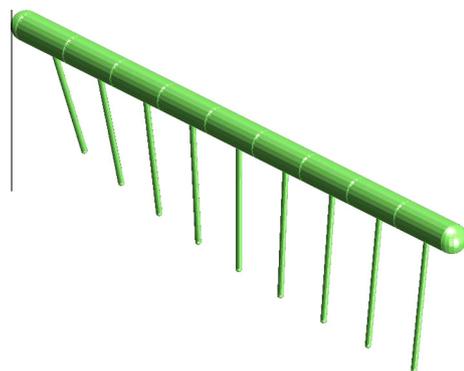

Fig. 2. Particle intra-element bending test: single particle, 9 elements, leftmost element fixed horizontally, other elements initially in line, gravity applied, particle oscillates and comes to rest; figure shows snapshot near greatest deformation in oscillation.

Fig. 3. Particle intra-element torsion test: single particle, 9 elements, zero gravity, zero translational velocity; far most element rotates about particle axis (anti-clockwise looking down axis from near end); thinner lines are not part of particle, they represent one of the element local axes and are seen to rotate about the particle axis; this example has a very soft torsional stiffness to illustrate the torsional deformation.

note on this criteria the stiffness is scaled with the particle mass – for further guidance on scaling and contact parameters in DEM see [11,12]. The particle damping is similarly scaled to give a constant damping coefficient reasonably representative of dried spaghetti. A typical friction coefficient has also been assigned (and a sensitivity study undertaken as shown later). Compared with most previous

Table 1
Principal DEM data for rigid particles.

Parameter	Value
Vessel height (m)	10
Vessel diameter (m)	0.21, 0.41, 0.61
Number of particles	500, 700, 700
Particle diameter (m)	0.01
Particle aspect ratio	10, 20, 30
Particle solid density (kg m^{-3})	2700
Particle elastic stiffness (N m^{-1})[a]	$1.4 * 10^5$
Contact damping coefficient	0.1
Contact friction coefficient	0.2
Time modelled (s)	10
Time step (s)	$4.1 * 10^{-5}$

Note no contact cohesion or rolling friction included.
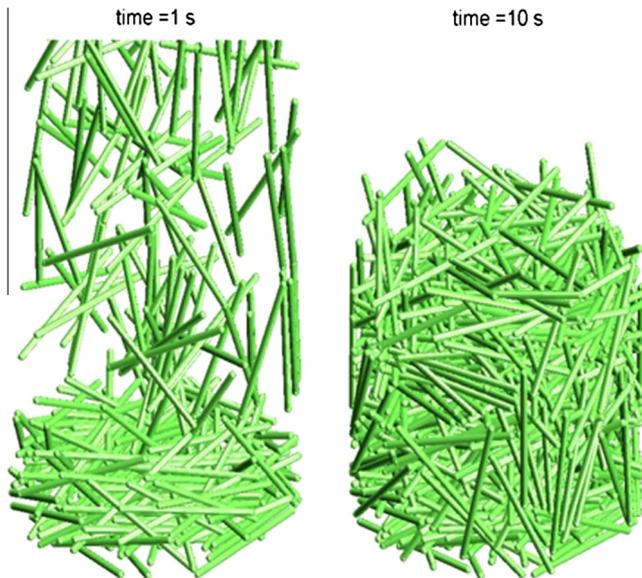
[a] Shown for $\lambda = 20$ only.

Fig. 4. Snapshots of DEM Sphero-cylinder fill and packing [9].

DEM cylinder simulations in the literature, this study models quite large aspect ratios. This poses some modelling challenges in obtaining stability. The principal data used is shown in Table 1 and example figures illustrating filling and packing are shown in Fig. 4. Initially all the particles are vertical and spaced out over a large height. As with any DEM simulation some randomness must be incorporated at the start to prevent unrealistic structure (e.g. spheres stacking in columns), and the fibres are given an initial downward velocity including a small random horizontal component. From Fig. 4 it can be seen that there is generally a distribution of particle orientations as they are falling. This study has not investigated the effect of initial state in detail; it is acknowledged that there could be some effects, but this study is considered representative of a fairly random loose orientation at bed impact for most particles.

In practice the particle would offer some flexure, whereas in this model it does not. The inflexible particles here, even with softened normal interactions, show ill-conditioned interactions due to "amplification" of motion – like a long lever with the fulcrum near one end. This is essentially overcome here by using the softened interaction, but also by limiting the particle angular velocity. In the filling stage the limit is set at 4π rad s^{-1}, and in the settling stage at 0.2π rad s^{-1}. The higher the aspect ratio the more "vulnerable" the system is to instability. Example packings for the largest aspect ratio $\lambda = 30$ are shown in Fig. 5, which show that stability is achieved. The significance of limiting angular velocity is considered further later.

3.2. Experimental study of packing to help validation

Experiments were undertaken at Nottingham dropping dried spaghetti, cut to specified aspect ratios, into a cylindrical vessel and measuring V_f (=1-voidage) as shown in Fig. 6. These show estimates of V_f for the particles simply dropped into the vessel and then for the vessel being tapped 20 times. Note the vessel diameter to particle length is significant here. The tapping also significantly improves packing. The spaghetti, with initially random orientations, are gradually poured through a funnel with a wide aperture (20 mm) causing approximate alignment of their long axis towards the vertical above the vessel. This makes it repeatable and reasonably representative of the method of fill used in the simulation described in Section 3.1 in giving a fairly general loose orientation for most particles impacting the assembly. Error bars show SD from a minimum of 6 repeats.

Parkhouse and Kelly [4] present a plot of solid volume fraction V_f vs. $1/\lambda$ for experimental data points and a theoretical curve; most of the experimental points lie just below the curve but follow its trend. The theoretical curve is applied in the following section to
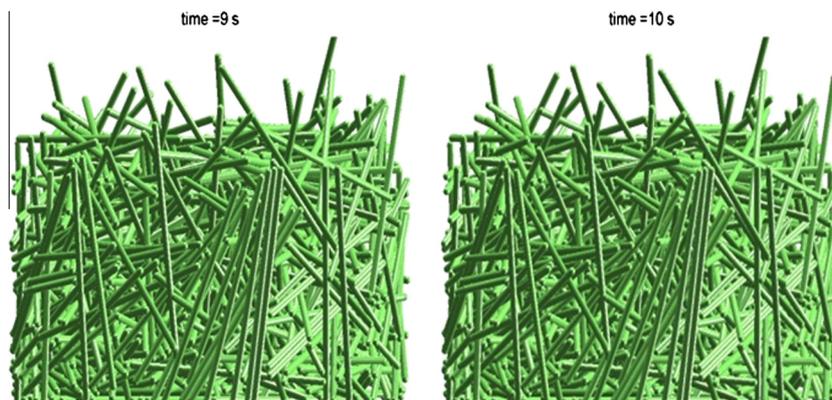

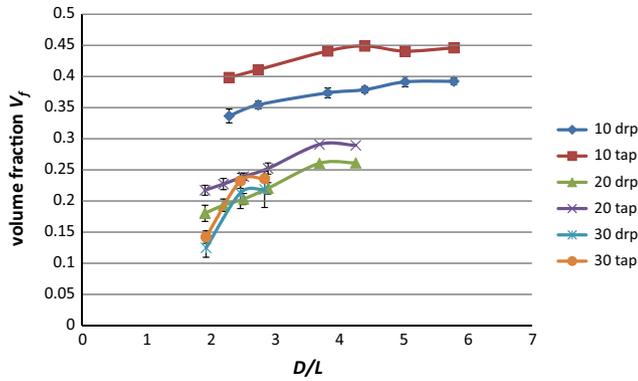**Fig. 5.** Stability achieved in DEM for $\lambda = 30$ [9].

Fig. 6. Experimental results of packing fraction for dried spaghetti; legend shows aspect ratio λ for particles dropped in vessel *drp* and then tapped *tap*; D is vessel diameter and L is particle length.

compare with our DEM results. Fig. 7 shows the range of our experimental values against theory [4]. It is interesting to note that the max values of the tapped cases are in very close agreement with the theory, which is an "optimised volume" case, leading to maximum packing. Most of the experimental data in [4] is indeed below the theoretical curve, and most within 0.04 of the curve, generally within the region of our tapped data.

3.3. DEM packing results for rigid particles

The simulation monitors two measures of solid volume fraction V_f: first on the whole vessel up to the centre of the highest particle;
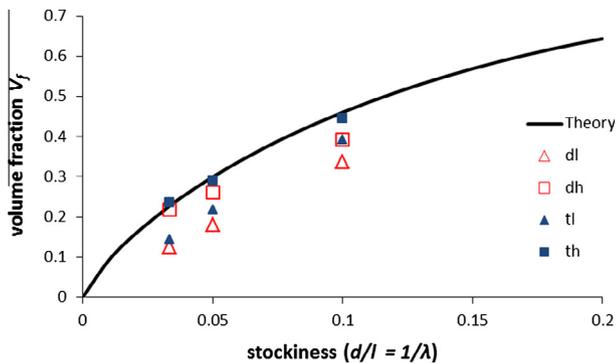
secondly in a cylindrical "sensor" region inside the packing about half the dimensions of the packing (1/8 volume), estimated numerically. The methods are illustrated schematically in Fig. 8. The values are close but the latter is taken as more representative of generic packing less dependent on the vessel size and wall effects; the extra runtime required for calculation of the latter is not significant overall. Fig. 9 shows results for the DEM simulations for λ = 10, 20, 30 and compares with the theory from [4]. These show good agreement. The DEM results are slightly lower than the theory as are most of the experimental cases cited in the reference. Indeed the DEM seems comparable with these experiments, and our experiments on tapped particles; note the simulation does not model tapping. The sensitivity of DEM packing fraction to friction (particle–particle and particle–wall) is shown in Table 2 for λ = 30; there is a significant variation but not major, which seems reasonable but is not experimentally validated here.

It is interesting to note the orientation distribution of the DEM settled packings shown in Fig. 10 for λ = 20 and 30. These are similar and show that most particles are near horizontal. This indicates that they have not been unduly restricted by the vessel walls during the filling. It would be useful to monitor this experimentally. The orientation is important from a material application viewpoint as it will control the isotropy in the sample; for example it might be fully 3D random, planar 2D random, possibly even significantly aligned in 1D, all of which could be desirable depending on the application/loading for the component.

Some further DEM simulations were undertaken varying D since our experiments noted some dependence of packing on D/L. These are for λ = 20 and are shown in Figs. 11 and 12 along with the relevant data from Fig. 6. There is some dependence in DEM
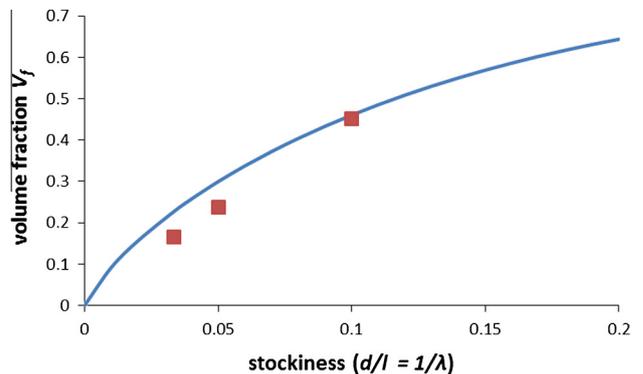

Fig. 7. Nottingham experimental results of packing fraction for dried spaghetti compared with theory [4]; *dl* is lowest of range for dropped fibres, *dh* is highest; *tl* and *th* are range for tapped fibres.

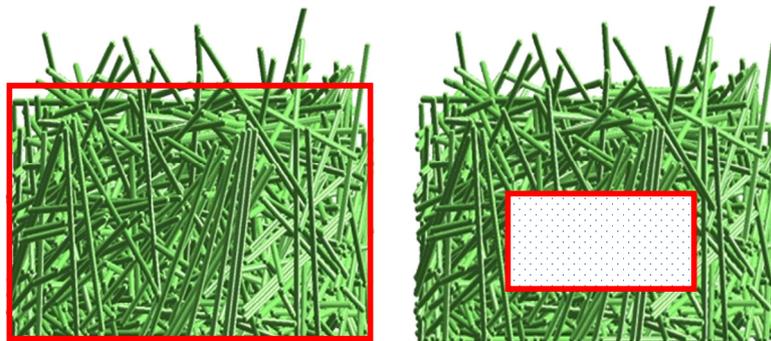**Fig. 9.** DEM results (squares) for sphero-cylinder packing compared with theory from [4].

Fig. 8. Principle of methods to calculate packing fraction: overall (left) based on highest particle centre to estimate bed volume; "sensor cell" region (right) based on assessing many equally spaced points in a cylindrical region away from edges, ie proportion of points inside any particle; particle spacing is about 0.01 of particle length. All of the results in this paper use the sensor region method unless otherwise stated.

Table 2
Sensitivity of packing fraction V_f to friction coefficient μ (particle–particle and particle–wall) for $\lambda = 30$.

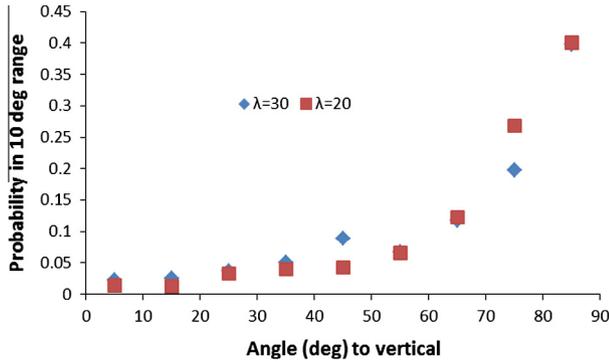| μ	V_f
0.1	0.179
0.2 (as plot)	0.162
0.3	0.155

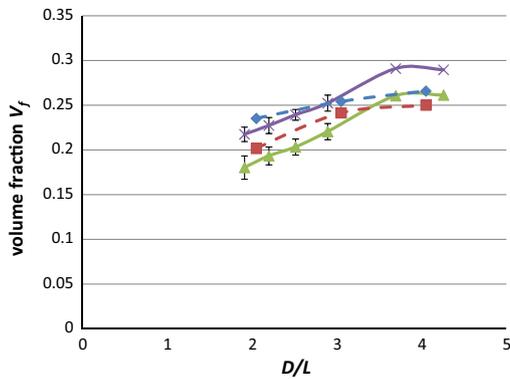**Fig. 10.** Particle orientation distribution in DEM.

Fig. 11. Experimental and DEM results of packing fraction for dried spaghetti for $\lambda = 20$; for experiment (solid line) particles dropped in vessel *drp* and then tapped *tap*; DEM (dashed line) for monitor cell and all vessel; D is vessel diameter and L is particle length. (As noted before DEM does not simulate the tapping.)

Fig. 12. Example DEM packing $\lambda = 20$, $D/L = 4$.

on D/L, but not as strong as in the experiment. This is probably because the DEM packing fraction is numerically estimated in a "sensor cell region" away from the walls, whereas the experiment is estimated from the overall assembly. This is somewhat supported by Fig. 11 which shows both the cell and overall DEM

results. (Results for some later simulations in Section 4.3 also indicate that the packing at the bed boundaries is lower than at the centre.)

4. Application of DEM to flexible fibre packing

4.1. Scenario and principal data

The above algorithm for connected sphero-cylinders (Section 2.4) is used here to model dropping flexible fibre particles into a cylindrical vessel to estimate the packing fraction. A similar scenario to Section 3 is modelled and most of the data is similar except that data is required to define the stiffness of the connections; Table 3 shows the principal data. An upper limit on angular velocity of 4π rad s^{-1} was set to help maintain stability for the largest aspect ratio particles. Initial simulations were undertaken with each particle modelled by one element and the results are close to those in Section 3 (stochastic features of the process lead to slightly different results). However, it is stressed that there is no experimental validation here for the flexible particle analysis and some of the data, such as for the flexure of the joints, is somewhat arbitrary, chosen to show some degree of flexure in the packing. Following the main set of simulations some further sensitivity runs were undertaken varying parameters on a base case which was taken as $\lambda = 20$, number of sub-elements per particle $N_{elem} = 3$.

4.2. Principal packing results for flexible particles

Fig. 13 shows example snapshots of the DEM simulation of the vessel filled with flexible particles for the base case $\lambda = 20$, $N_{elem} = 3$; these show the particles have settled and are stable. Fig. 14 shows some examples for the larger fibres. (Carbon fibres are a potential application here.) The flexibility at the sub-elements joints is clearly visible for these cases. Table 4 shows the resulting packing fractions from the simulations for different aspect ratios and number of sub-elements; these are numerically "measured in a sensor region" as in Section 3. The table also shows for comparison the equivalent theoretical values [4] and the simulation results in Section 3 for rigid particles. As stated above the results for $N_{elem} = 1$ are consistent with Section 3. With an increase of N_{elem} to 3, a larger packing fraction is clearly achieved in all cases, i.e. allowing a particle to deform into the free space, which is intuitively reasonable. However, for a further increase of N_{elem} to 5 the trend is not clear. It should be noted that as N_{elem} increases the joint bending and torsional stiffness increase (see Appendix A) so that the overall particle has similar flexure as shown in Fig. 14 and the packing structure does not look significantly different. Fig. 15 shows the settled particles for $\lambda = 10$ $N_{elem} = 3$ and 5;

Table 3
Principal DEM data for flexible particles.

Parameter	Value
Vessel height (m)	10
Vessel diameter (m)	0.21, 0.41, 0.61
Particle aspect ratio	10, 20, 30
Number of particles	400, 1000, 1200
Particle diameter (m)	0.01
Particle solid density (kg m^{-3})	2700
Particle elastic stiffness (N m^{-1})[a]	$4.7 * 10^4$
Contact damping coefficient	0.1
Contact friction coefficient	0.2
Time modelled (s)	Up to 15
Time step (s)	$4.1 * 10^{-5}$
Number of elements/particle	1, 3, 5
Joint bending stiffness etc	See Appendix A

[a] Shown for base case only.

time =8.998 s   time =9.998 s

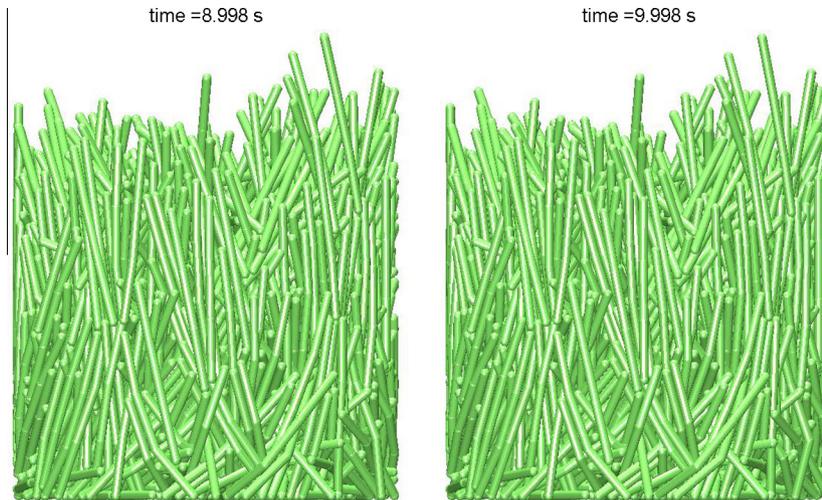**Fig. 13.** Example of "Base Case" for flexible fibres with 1000 particles, λ = 20, N_{elem} = 3, showing stable filled vessel.

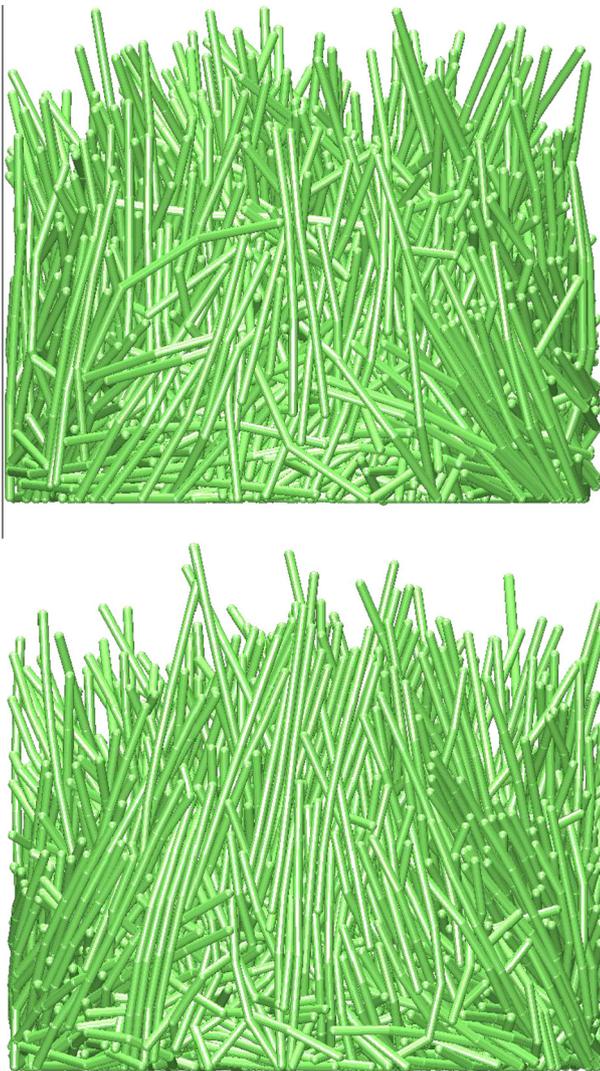**Fig. 14.** Example of filled vessel with 1200 flexible particles, λ = 30, N_{elem} = 3 top, =5 lower.

Table 4
Packing fraction V_f vs. aspect ratio λ for theory, rigid model in Section 3, flexible model for different no. elements N_{elem} in each particle.

λ	Theory [4]	Section 3	N_{elem} = 1	N_{elem} = 3	N_{elem} = 5
10	0.461	0.452	0.457	0.525	0.496
20	0.300	0.238	0.235	0.361	0.398
30	0.227	0.165	0.180	0.310	0.261

there is probably not a significant change in packing beyond N_{elem} = 3 given that overall flexure is reasonably constant.

The orientation distribution of the settled packings are shown in Fig. 16 for λ = 20 and 30 for N_{elem} = 3; these are based on central element of particle. These are significantly different to the rigid particle cases in Section 3 and show that particle central elements are less aligned to the horizontal. Fig. 14 shows example graphics for the settled particles for λ = 30. Particle flexibility has enabled a greater packing fraction and a more general orientation with less overall alignment.

4.3. Sensitivity study for flexible particles

To test the robustness of some aspects of the model and to examine the sensitivity of certain parameters some further simulations were undertaken on the base case as mentioned in Section 4.1. First some simulations were repeated with different (±20%) initial particle velocities u_0 for λ = 20 N_{elem} = 3 to replicate "repeated lab experiments", ie the initial velocity should have no significant effect, any variation would be purely stochastic; Table 5 shows the solid volume fraction V_f varies moderately with no trend. The variation is consistent with our repeated experiments shown in Fig. 6. It may be that a larger system with larger monitoring region would have less stochastic variation, but run times would be larger. However, with this particular configuration it was noted that the cell size could indeed be increased by doubling its height and still remain clear of edge effects at the top of the bed. Further results in Table 5 do indeed show less stochastic variation for the larger cell. Note these also show the more approximate voidage estimated from the first method of Fig. 8 for the overall bed. As expected these indicate lower packing at the boundaries.

From a modelling perspective a significant question remains as to the necessity to limit the maximum angular velocity ω_L of the particles. It was noted that the flexible particles continue to be stable when the limit is increased. For example the base case could be run with ω_L = 12π rad/s (3 times base case value) and still give a
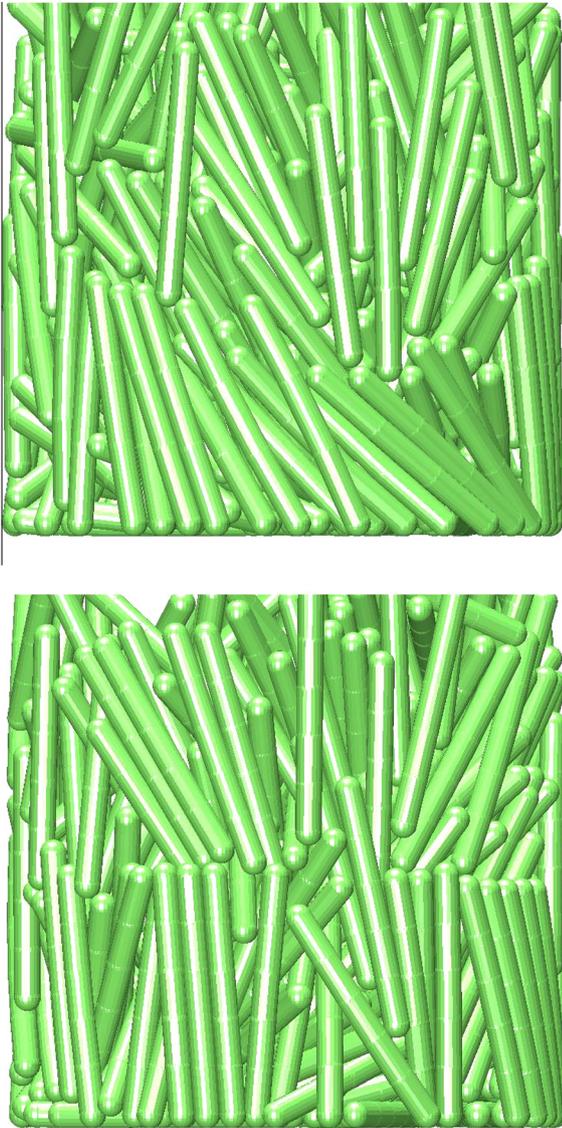
again no obvious difference in structure is evident. The simulations were repeated for N = 500 and gave very similar results. Hence

Fig. 15. Settled flexible particles for λ = 10, N_{elem} = 3 top, =5 lower.

Fig. 16. Flexible particle orientation distribution in DEM based on central element of each particle.

Table 5
Sensitivity of packing fraction V_f to initial particle velocity u_0.

u_0 (cm/s)	V_f initial cell	V_f larger cell	V_f overall bed
0.8 * 40	0.382	0.377	0.302
40 (base case)	0.361	0.370	0.294
1.2 * 40	0.398	0.393	0.323

Table 6
Sensitivity of packing fraction V_f to particle elastic stiffness k.

k (N/m)	V_f larger cell	V_f overall bed
0.5 * base case	0.374	0.305
$4.7 * 10^4$ (base case)	0.370	0.294
2 * base case	0.359	0.314

Table 7
Sensitivity of packing fraction V_f to particle friction coefficient μ (p–p and p–w).

μ	V_f larger cell	V_f overall bed
0.1	0.412	0.368
0.2	0.370	0.294
0.4	0.324	0.259

efficiency, but given the stable, consistent and realistic results as regards packing fraction this paper shows the feasibility of the model.

Simulations were undertaken varying the particle elastic stiffness k, both normal and tangential which are set to be the same. These were on the base case with the larger monitor cell noted above. Table 6 shows minimal variation consistent with the "repeated experiments" above. This adds confidence to the simplified contact model used here which has also been experimentally verified in previous studies e.g. [7]. There was some significant variation in packing fraction for friction coefficient change as shown in Table 7. As for the rigid particles, the lower the friction the greater the packing fraction as expected.

Some further simulations, details omitted for brevity, indicate that packing fraction is not highly sensitive to 50% changes in joint flexibility.

5. Conclusions

5.1. Rigid fibres

– DEM is applied to model packing of sphero-cylinders in a cylindrical vessel. Conventional methods are used with softened contact interactions. The aspect ratio is quite large for DEM which caused some stability issues. Use of softened interactions as commonly applied to enable a reasonable timestep and limiting angular velocity allowed stable packings up to λ = 30.
– DEM results of V_f vs. λ showed very good agreement with information in the literature, including experimental and theoretical data [4]. There was some significant dependence of packing on friction in the DEM.
– Particle orientation in the DEM showed that most particles are close to horizontal. It would be useful to analyse experimental data on this.

5.2. Flexible fibres

– The model was developed to include particle flexure by linking sphero-cylinders, referred to as sub-elements, with translational, bending and torsional stiffness, at the joints. Various "debugging" tests were undertaken to show appropriate

stabled settled bed with similar voidage, however, at higher values the simulation can be terminated due to the maximum particle overlap criterion being exceeded. An alternative would be to reduce the time step of the simulation, but then of course the CPU time increases which is one of the limitations of DEM. This is a potential future study along with increasing the code

bending and torsion in idealised single particle systems. The model was also tested with single sub-element particles which essentially reproduced the rigid particle case results.

– Increasing the No. sub-elements per particle from 1 to 3 significantly increased the packing fraction and also gave rise to a more general particle orientation based on the central element. Further increases in the No. elements had little effect because the joint flexibility was correspondingly decreased giving the particle the same overall flexure.

– The numerical simulation is more stable with flexible particles but limiting angular velocity is still required in the simulations undertaken here which appear to give reasonable results. Possibly reducing the timestep and modelling more sub-elements would negate this requirement.

– As with the rigid particles, particle packing fraction shows some significant variation for friction. It does not vary significantly with 50% changes in particle elastic stiffness as expected, supporting the use of the simplified contact model.

– The current model would not be suitable in certain situations such as where interstitial fluid has a significant effect, where there is excessive bending so a particle "contacts itself", or where a straight fibre would buckle due to high end loading.

– The program has potential for flexible fibre applications, but standard techniques should be used to speed up the processing such as zoning and near-neighbour lists applied to the particle sub-elements.

Acknowledgements

Appendix A. Intra-particle joint translational, bending and torsional stiffness

A.1. Translational

Each particle can be considered as a series of connected sub-elements which are sphero-cylinders. A joint is a shared sphere, but as the particle deforms the joint effectively has two overlapping spheres; a linear restoring force is applied to pull the sphere centres together; the joint stiffness is the same as the particle contact stiffness k, which is set to allow a maximum particle–particle overlap of about $0.05d$ under the greatest loading conditions (usually on initial impact with the base not in the final packed state where it is much less); k is scaled by the mass of the particle sub-element in each simulation for reasons described in Section 3.1.

A.2. Bending and torsional

The equations below have been taken from Benham and Warnock [19]. Material data has been taken for this study as 1%

of values given for Perspex ($E = 2.8e9$ Pa, $G = 1e9$ Pa). This was taken on a trial and error basis to model some reasonably flexible fibres. Angular damping is taken as 10% of critical damping, similar to the normal contact damping.

$$M = \frac{EI}{L_e} \theta_b \tag{A1}$$

$$T = \frac{GJ}{L_e} \theta_{tr} \tag{A2}$$

$$I = \frac{\pi d^4}{64} \tag{A3}$$

$$J = \frac{\pi d^4}{32} \tag{A4}$$

where d is the particle diameter, E is Young's modulus, G is Shear modulus, I is second moment of area, J is polar second moment of area, L_e is particle sub-element length, M is moment, T is torque, θ_b bending angle between two connected elements, θ_{tr} is the torsion angle between two connected elements.

References

[1] M.J. Starink, S. Syngellakis, Mater. Sci. Eng. A – Struct. 270 (2) (1999) 270–277, http://dx.doi.org/10.1016/S0921-5093(99)00277-4.

[2] J.W. Kaczmar, K. Pietrzak, W. Wlosinski, J. Mater. Process. Tech. 106 (1–3) (2000) 58–67.

[3] D.B. Miracle, Compos. Sci. Technol. 65 (15–16) (2005) 2526–2540.

[4] J.G. Parkhouse, A. Kelly, P R Soc. Math. Phys. Sci. 451 (1943) (1995) 737–746, http://dx.doi.org/10.1098/rspa.1995.0152.

[5] A. Dziugys, B. Peters, Granul. Matter. 3 (4) (2001) 231–265, http://dx.doi.org/10.1007/Pl00010918.

[6] P.A. Langston, M.A. Al-Awamleh, F.Y. Fraige, B.N. Asmar, Chem. Eng. Sci. 59 (2) (2004) 425–435, http://dx.doi.org/10.1016/j.ces.2003.10.008.

[7] S. Mack, P. Langston, C. Webb, T. York, Powder Technol. 214 (3) (2011) 431–442, http://dx.doi.org/10.1016/j.powtec.2011.08.043.

[8] B.N. Asmar, P.A. Langston, A.J. Matchett, J.K. Walters, Comput. Chem. Eng. 26 (6) (2002) 785–802.

[9] P. Langston, A. Kennedy, H. Constantin, Discrete element modelling of high aspect ratio sphero-cylinder particle packing, in: Paper Presented at the III International Conference on Particle-based Methods – PARTICLES 2013, Stuttgart, Germany, 18–20 September, 2013.

[10] Y.C. Zhou, B.H. Xu, A.B. Yu, P. Zulli, Powder Technol. 125 (1) (2002) 45–54. pii: S0032-5910(01)00520-4, doi: 10.1016/S0032-5910(01)00520-4.

[11] Y.T. Feng, K. Han, D.R.J. Owen, J. Loughran, Eng. Comput. 26 (6) (2009) 599–609, http://dx.doi.org/10.1108/02644400910975405.

[12] K.F. Malone, B.H. Xu, Particuology 6 (6) (2008) 521–528, http://dx.doi.org/10.1016/j.partic.2008.07.012.

[13] R. Cruz Hidalgo, L. Zuriguel, D. Maza, I. Pagonabarraga, Phys. Rev. Lett. 103 (11) (2009). Artn 118001, doi: 10.1103/Physrevlett.103.118001.

[14] R.C. Hidalgo, D. Kadau, T. Kanzaki, H.J. Herrmann, Granul. Matter. 14 (2) (2012) 191–196, http://dx.doi.org/10.1007/s10035-011-0303-2.

[15] Wenguang Nan, Yueshe Wang, Yuan Ge, Jianzhong Wang, Powder Technol. 261 (2014) 210–218.

[16] Y. Guo, C. Wassgren, B. Hancock, W. Ketterhagen, J. Curtis, Powder Technol. 249 (2013) 386–395, http://dx.doi.org/10.1016/j.powtec.2013.09.007.

[17] Y. Sheng, D.M. Yang, Y.Q. Tan, J.Q. Ye, Compos. Sci. Technol. 70 (14) (2010) 2093–2101, http://dx.doi.org/10.1016/j.compscitech.2010.08.006.

[18] D.M. Yang, Y. Sheng, J.Q. Ye, Y.Q. Tan, Comp. Mater. Sci. 49 (2) (2010) 253–259, http://dx.doi.org/10.1016/j.commatsci.2010.05.003.

[19] P.P. Benham, F.V. Warnock, Mechanics of Solids and Structures, Pitman Publishing, 1973.